Macromolecules

ARTICLE

pubs.acs.org/Macromolecules

# Manipulation on the Morphology and Electrical Properties of Aligned Electrospun Nanofibers of Poly(3-hexylthiophene) for Field-Effect Transistor Applications

Jung-Yao Chen,[⊥,†] Chi-Ching Kuo,[⊥,‡] Chia-Sheng Lai,[§] Wen-Chang Chen,[*,†,‡] and Hsin-Lung Chen[*,§]

[†]Department of Chemical Engineering, National Taiwan University, Taipei, Taiwan

[‡]Institute of Polymer Science and Engineering, National Taiwan University, Taipei, Taiwan

[§]Department of Chemical Engineering, National Tsing Hua University, Hsin-Chu, Taiwan

Supporting Information

**ABSTRACT:** We prepared aligned poly(3-hexylthiophene) (P3HT) nanofibers for the application of organic field-effect transistor (OFET) by two-fluid coaxial electrospinning (ES) technique using P3HT as core and PMMA as shell, followed by extraction of PMMA. Effects of shell flow rate and thermal annealing temperature on the morphology and optoelectronic properties were explored. The experimental results showed that the prepared P3HT nanofibers were highly aligned and their diameters were smaller in the case of low shell flow rate. The OFET carrier mobility of aligned P3HT ES nanofibers using the low shell flow rate could be dramatically improved up to 3 orders of magnitude ($1.92 \times 10^{-1}$ cm$^2$/V·s with the on/off ratio of $4.45 \times 10^4$) in comparison with those from the high shell flow rate. The results of wide-angle X-ray scattering (WAXS) and photophysical properties (optical absorption and polarized photoluminescence) suggested the enhancement of $\pi-\pi$ stacking and crystallinity of P3HT in the nanofibers at a lower shell flow rate, due to the higher electrical force along nanofiber axis. Besides, as thermal annealing temperature was higher than 100 °C, the relaxation of P3HT orientation in the nanofibers led to a reduction of the measured field-effect mobility. The experimental results addressed the importance of the process parameters (i.e., the shell flow rate and thermal annealing temperature) on tuning the chain packing and orientation of P3HT in nanofibers and the resultant OFET characteristics.

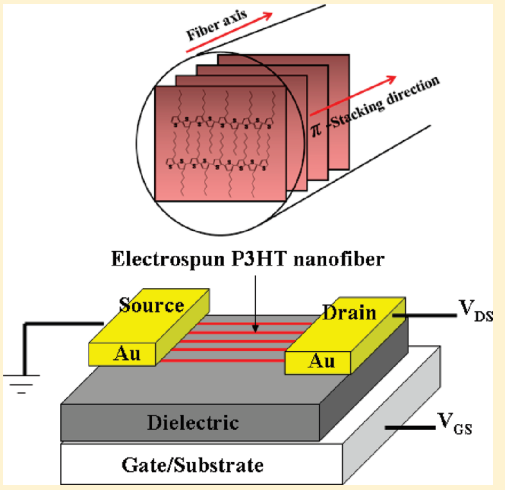


## INTRODUCTION

Regioregular poly(3-alkylthiophenes) (P3HT) have attracted extensive scientific interest due to their superior charge-transporting characteristics and favorable processability for optoelectronic device applications, such as photovoltaic cells (PV)[1−4] and organic field-effect transistor (OFET).[5−9] Aligned one-dimensional (1D) structure with nanometer-sized confinement would significantly enhance the orientation of P3HT crystals, which is more favorable for its anisotropic charge transport than the unaligned 1D structure. The charge-carrier mobility of P3HT OFET could be manipulated over a wide range of $4 \times 10^{-4}$ to $3 \times 10^{-2}$ cm$^2$/V·s through different nanostructure or orientation on crystal domains, such as nanofibers.[10−15]

P3HT nanofibers were generally produced via solution self-assembly[11,12] or electrospinning (ES).[13−15] We are particularly interested in producing polymer nanofibers through the ES process because it has the advantages of low cost, flexible morphology tuning, and high-throughput continuous production.[16−20] The strong stretching force and the geometrical confinement associated with the ES process could induce the orientation of polymer chains along the long axis of fiber,[21−23] whose photoelectronic properties were different from that in the spin-coated films.[24−31] In addition, ES aligned nanofibers were easily prepared from several approaches,[32−38] including a scanning tip,[32] a drum rotating at a high speed,[33] a rotating wheel-like bobbin,[34] collector/electrode modification,[22,35,36] and magnetic field-assistance.[37] Liu et al. prepared single P3HT ES nanofiber-based OFET with the mobility as high as 0.03 cm$^2$/V·s.[14] However, droplets and beaded P3HT nanofibers were occasionally formed due to the rapid evaporation of the solvent and low polymer solubility. Recently, Lee et al. used the coaxial setup to produce continuous and uniform P3HT ES nanofibers with the carrier mobility of 0.017 cm$^2$/V·s, by continuously providing solvent in the shell to prevent the phase separation of P3HT from the solution at the end

**Received:** October 5, 2010
**Revised:** March 14, 2011
**Published:** March 25, 2011

ACS Publications © 2011 American Chemical Society

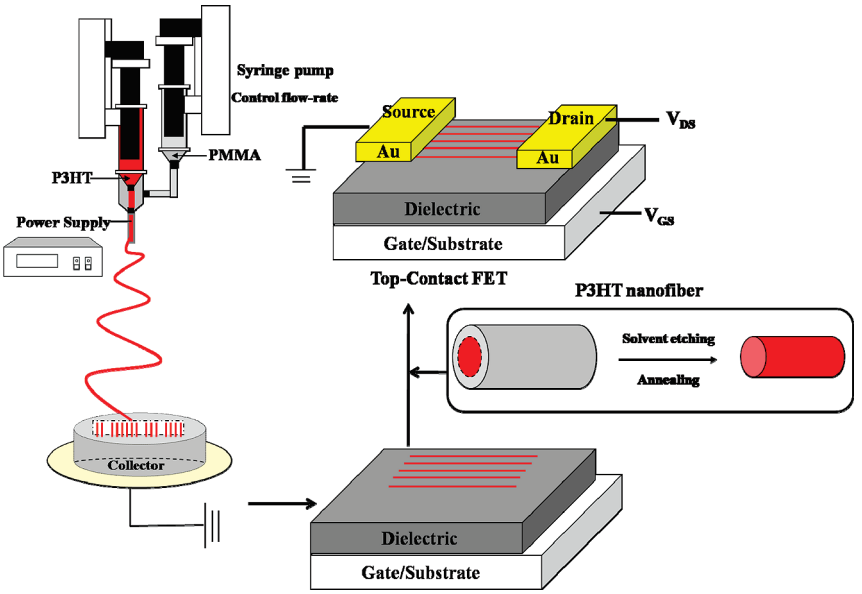


**Figure 1.** Schematic representation of the coaxial electrospinning setup and process to fabricate the aligned ES P3HT nanofiber based OFET.

of the nozzle.[13] This group further reported higher-performance P3HT ES nanofiber-based OFET by replacing traditional silicon oxide with polyelectrolyte gate dielectric and reached a high mobility of 2.0 $cm^2/V \cdot s$ and the on/off current ratio of $10^5$.[38] Nevertheless, manipulating the P3HT crystalline structure and orientation within the ES nanofibers for device applications has not been fully explored. It has been reported that the morphology and charge-carrier mobility of P3HT spin-coated films could be significantly modified by the processing solvent and annealing temperature.[5,8,39] However, such manipulation on P3HT ES nanofibers and their related device characteristics require further exploration.

Herein, we prepared aligned P3HT nanofiber-based OFET by a two-fluid coaxial ES technique consisting of P3HT core and PMMA shell followed by extraction of PMMA, as schematically illustrated in Figure 1. Instead of using the solvent in the shell,[13] the PMMA polymer solution as shell flow could easily tune the P3HT core diameter and also prevent the doping of P3HT nanofibers by oxygen. The effects of shell flow rate and annealing temperature on the morphology and carrier mobility of the P3HT ES nanofibers were examined here. The morphology of the prepared nanofibers was characterized by field-emission scanning electron microscope (FE-SEM), wide-angle X-ray scattering (WAXS), fluorescence optical microscope, and atom force microscopy (AFM). Optical absorption and polarized photoluminescence were used to explore P3HT chain packing in the nanofibers. Our experimental results indicate that the crystallinity and orientation of P3HT ES nanofibers could be tuned by the process parameters for high-performance OFET applications.

## EXPERIMENTAL SECTION

**Materials.** P3HT ($M_w \sim 50\,000$, 90−95% regioregular) was used as received from Reike Metals Inc. (Lincoln, NE). PMMA ($M_w \sim 350\,000$) was purchased from Sigma-Aldrich (Milwaukee, WI). Tetrabutylammonium perchlorate (TBAP, TCI (Tokyo, Japan)) and Octadecyltrichlorosilane (ODTS, Sigma-Aldrich) were used as received without further purification. Chlorobenzene (CB; anhydrous 99.8%) was purchased from Sigma-Aldrich.

**Electrospinning (ES) Process.** A two-fluid coaxial ES technique[24,25,29] with collector modification[30,35,36] was used to produce aligned core−shell nanofibers, as shown in Figure 1. As exhibited in the figure, two syringes containing core and shell precursor solutions were used for producing the ES nanofibers. Note that each syringe was connected to a separate needle, and the needle was placed one inside the other to form a two-fluid coaxial ES system. 50 mg/mL of P3HT as core solution was dissolved in anhydrous chlorobenzene (CB) overnight under $N_2$-filled glovebox. 300 mg/mL of PMMA as shell solution was dissolved in anhydrous CB with 10 wt % of TBAP added to increase conductivity and stabilize the cone-jet.[30,36] The two solutions were fed into the coaxial capillaries by two syringe pumps (KD Scientific Model 100, USA). The feed rate of P3HT solution (core flow) was fixed at 0.1 mL/h while the feed rates of PMMA solution (shell flow) was operated at 0.5, 1.0, 1.5, and 2.0 mL/h, respectively. The tip of the core needle was connected to a high-voltage power supply (chargemaster CH30P SIMCO, USA). The spinning voltage was set at 9.7−11.9 kV. The collector made of electrically charged conductive aluminum disk (diameter 7 cm, high 1.5 cm) with a rectangular hole (4 cm in length and gap width of 1 cm) was placed 13 cm below the tip of the needle (working distance) to collect the aligned nanofibers, similar to our previous report[30,36] and the other literature.[35] The fiber alignment could be controlled by the following two factors:[30,35,36] (1) the electrostatic force between positive-charged fibers and negative charge of gap edge stretches the fibers across the gap, as shown in Figure 1; (2) the electrostatic repulsion between the deposited and upcoming fiber further enhances the parallel alignment. The ES process system must keep in stable cone-jet spinning mode observed by CCD camera (Xli 3 M USB2.0 CCD camera, USA) and Macro video zoom lens (OPTEM MVZL, USA) for obtaining uniform and aligned fibers. All experiments were carried out under ambient environment.

**OFET Device Fabrication.** As shown in Figure1, highly aligned coaxial P3HT(core)/PMMA(shell) ES nanofibers produced from the above ES process and then transferred from collector to the silicon wafer with thickness 200 nm of $SiO_2$ used as a gate dielectric. With the aim to immobilize the P3HT nanofibers during solvent extraction and reduce the defects on the substrates, the substrates were obtained by the following procedures: a heavily n-type doped wafer was immersed into piranha

**Table 1. Fiber Diameters and Electrical Properties of the P3HT ES Nanofibers Based OFET Devices Prepared at Different Process Parameters**

| sample | shell flow rate (mL/h) | annealing temperature (°C) | Fiber diameter[b] (nm) | $\mu_{max}$[c] ($cm^2/V \cdot s$) | $I_{on/off}$ (−) | $V_{TH}$ (V) |
|---|---|---|---|---|---|---|
| **PHTNF-1** | 0.5 | 100 | 168 ± 20 | $1.78 \times 10^{-1}$ | $7.54 \times 10^{2}$ | 3.3 |
| **PHTNF-2** | 1 | 100 | 131 ± 15 | $1.92 \times 10^{-1}$ | $4.45 \times 10^{4}$ | 0.8 |
| **PHTNF-3** | 1.5 | 100 | 257 ± 23 | $5.93 \times 10^{-4}$ | $1.17 \times 10^{3}$ | 3.3 |
| **PHTNF-4** | 2 | 100 | 520 ± 34 | $2.60 \times 10^{-4}$ | $1.65 \times 10^{3}$ | 10 |
| **PHTNF-5** | 1 | w/o[a] | 325 ± 21 | $1.51 \times 10^{-4}$ | $2.78 \times 10^{1}$ | 14.3 |
| **PHTNF-6** | 1 | 50 | 124 ± 10 | $5.56 \times 10^{-2}$ | $1.25 \times 10^{6}$ | −0.5 |
| **PHTNF-7** | 1 | 150 | 442 ± 31 | $4.57 \times 10^{-2}$ | $1.15 \times 10^{2}$ | 10 |
| **PHTNF-8** | 1 | 200 | 421 ± 33 | $4.88 \times 10^{-3}$ | $1.66 \times 10^{3}$ | 7.5 |

[a] w/o.: without annealing. [b] Average fiber diameter estimated from more than three nanofibers. [c] The highest charge carrier mobility obtained from measuring at least three OFET devices (Table S1, Supporting Information).

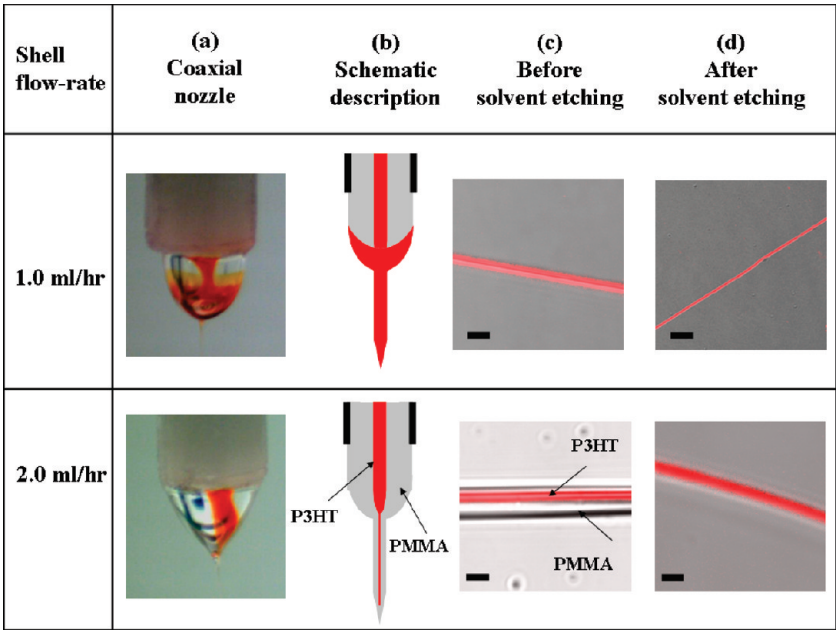


**Figure 2.** (a) CCD images and (b) schematic description on the stable cone-jet spinning model during two-fluid coaxial ES process at different shell flow rates: 1.0 mL/h (**PHTNF-2**) and 2.0 mL/h (**PHTNF-4**). Confocal images of **PHTNF-2** and **PHTNF-4** (c) before and (d) after solvent etching (the size of all scale-bars is 2 $\mu$m).

solution (volume ratio 7:3 of $H_2SO_4$ and $H_2O_2$) to remove the organic impurities and obtain OH-groups on the surface. Then, the $SiO_2$ were treated by surface treatment agent of octadecyltrichlorosilane (ODTS). The silane was added to the flask (3.94 $\mu$L/ml in anhydrous toluene), and left to self-assemble on the substrates for 1 h under $N_2$-filled glovebox in order to minimize the trace amounts of water reacted with silane.

Aligned coaxial P3HT(core)/PMMA(shell) ES nanofibers located on the above $SiO_2$/Si substrates were immersed in acetone for 1 h to extract the PMMA shell layer and then dried . After drying, these samples were annealed at 50, 100, 150, and 200 °C for 20 min to explore the thermal effect. Thermal annealing was carried out on a calibrated and stabilized hot plate under vacuum. After annealing, all the devices were placed on hot plate at room temperature to cool down. The top-contact source and drain electrodes were defined by 350 nm-thick of gold through a regular shadow mask, and the channel length ($L$) and width ($W$) were 25 and 1500 $\mu$m. In this study, P3HT ES nanofibers prepared from various processing parameters are denoted **PHTNF-1**∼ **PHTNF-8** and their characteristics are listed in Table 1.

**Characterization.** The morphology of the prepared ES nanofibers was characterized by the following instruments. The field-emission scanning electron microscope FE-SEM (JEOL JSM-6330F) images were taken using a microscope operated at an accelerating voltage of 10 kV. Before imaging, the samples were sputtered with Pt. Internal molecular structure in pure P3HT ES nanofibers after annealing was investigated by transmission-mode X-ray diffraction (XRD) at beamline 17A and 01C of National Synchrotron Radiation Research Center, Taiwan. Optical micrograph under cross polarizers was used to detect the orientation characteristics of ES fibers. Atomic force micrographs of the P3HT ES nanofibers were obtained with a Nanoscope 3D Controller AFM (Digital Instruments, Santa Barbara, CA) operated in the tapping mode at room temperature. Commercial silicon cantilevers (Nanosensors, Germany) with typical spring constants 21−78 N/m was used and the images were taken continuously with the scan rate of 1.0 Hz.

Fluorescence optical microscope images were taken using two photon laser confocal microscope (Confocal) (Leica LCS SP5). Optical absorption spectra for ES nanofibers were recorded using the UV−visible spectrophotometer (Hitachi U-4100). Polarized steady-state luminescence was recorded on polarizers for the Spex-Fluorolog-3 spectrofluorometer system (Horiba Jobin Yvon), as described in our previous study.[30,36] Output and transfer characteristics of the P3HT ES

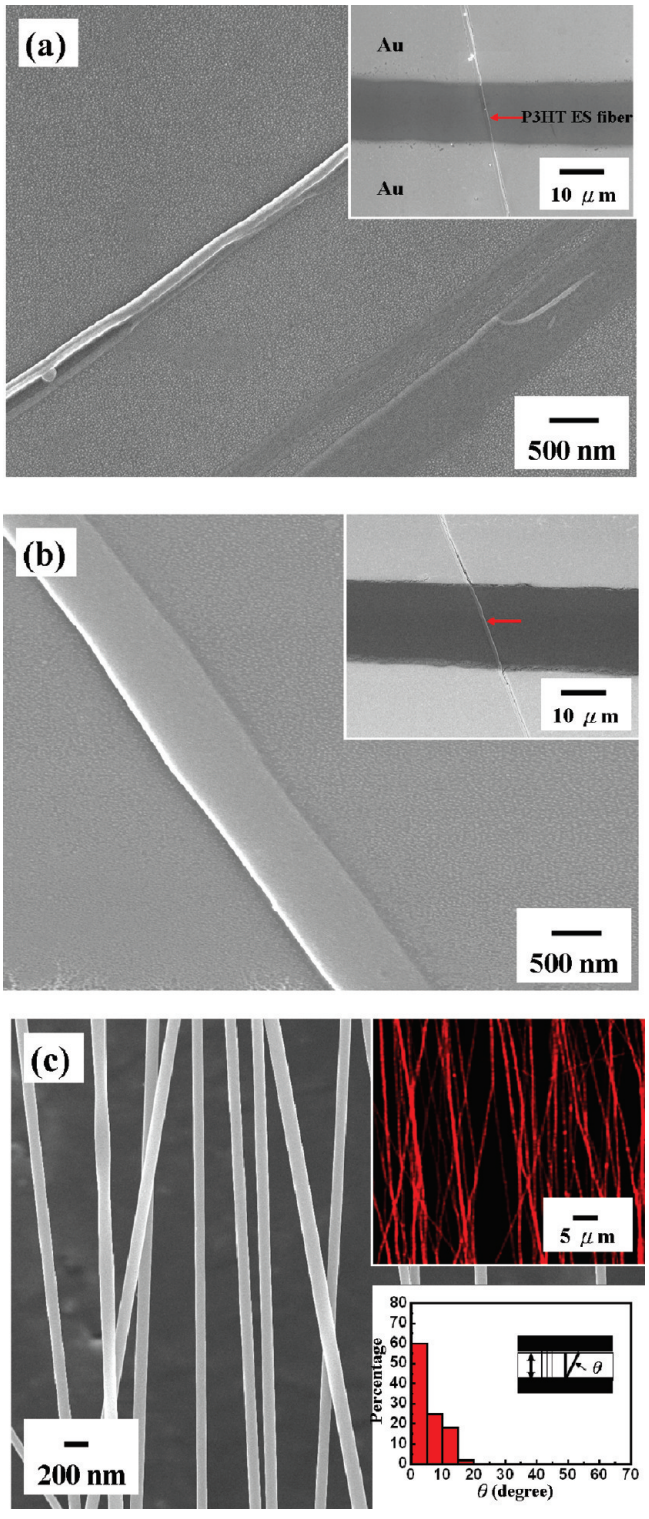


**Figure 3.** FE-SEM images of (a) **PHTNF-2** and (b) **PHTNF-4**. The inset FE-SEM figures show the typical transistor of the above P3HT nanofibers. (c) FE-SEM images and confocal images of **PHTNF-2**. The inset figures show that distribution of the angle between the long axis of a fiber and the normal to the edges of two parallel aluminum plates. The results displayed in each plate came from measurements on more than 50 fibers.

nanofibers based OFET devices were measured using Keithley 4200 semiconductor parametric analyzer. The above electrical measurements were performed in a nitrogen-filled glovebox.

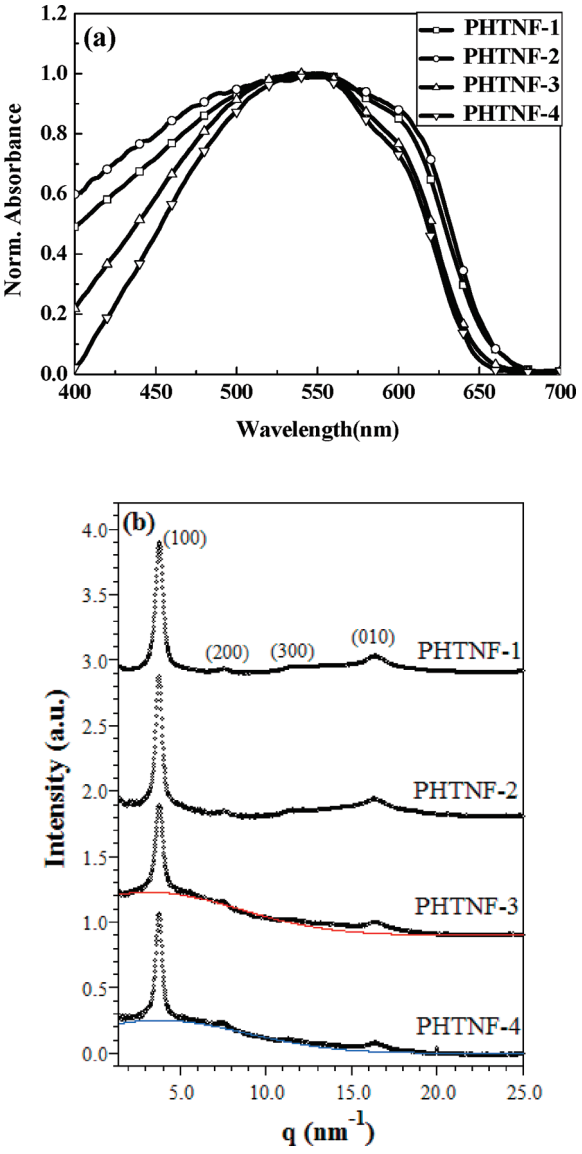


**Figure 4.** (a) Optical absorption spectra of **PHTNF-1**, **PHTNF-2**, **PHTNF-3**, and **PHTNF-4**. (b) WAXS patterns of **PHTNF-1**, **PHTNF-2**, **PHTNF-3**, and **PHTNF-4** after solvent etching and annealing. The broad peak beneath the (100) diffraction peak in the profiles of **PHTNF-3** and **PHTNF-4** was shown by the Gaussian curves that fit along the baselines of the data.

## RESULTS AND DISCUSSION

**Effect of Shell Flow Rate.** *Morphology.* Parts a and b of Figure 2 show the CCD images and schematic description of the stable cone-jet ES process at different PMMA shell flow rates of 1.0 (**PHTNF-2**) and 2.0 mL/h (**PHTNF-4**), respectively, while fixing the P3HT core flow rate at 0.1 mL/h. Also, the confocal images of the above ES nanofibers before and after solvent etching are shown in parts c and d of Figure 2, respectively. In the case of the lower shell flow rate, the P3HT core solution (red color) diffusing to the PMMA shell is more significant and thus P3HT solution accumulated on the tip of the cone, as shown in parts a and b of Figure 2. Therefore, the confocal image of **PHTNF-2** emits red color within the entire ES nanofibers before solvent etching but that of the **PHTNF-4** exhibits a core−shell

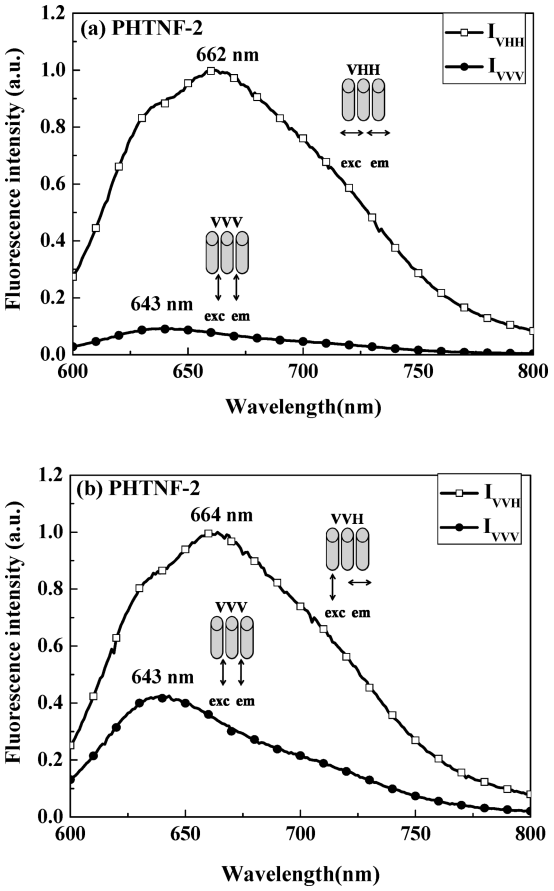


**Figure 5.** Polarized photoluminescence of aligned **PHTNF-2** (a) with exciting light and emission collected polarized perpendicular to the fiber axis ($I_{VHH}$) and with exciting light and emission collected polarized parallel to the fiber axis ($I_{VVV}$) (b) with exciting light polarized parallel to the fiber axis, and emission collected polarized perpendicular ($I_{VVH}$) and parallel ($I_{VVV}$) to fiber axis.

structure. It suggests that the strong shear force between shell and core boundary at the higher shell flow rate could prevent P3HT diffusing into the PMMA shell. The average fiber diameters of **PHTNF-2** and **PHTNF-4** before etching are 2.27 and 3.53 $\mu$m, respectively, as measured from the FE-SEM images (Figure S1). After solvent etching, the fiber diameter of **PHTNF-2** is significantly decreased to 131 $\pm$ 15 nm because P3HT diffused into PMMA shell is etched out, as exhibited in Figure 3a. On the other hand, **PHTNF-4** could retain the P3HT core/PMMA shell structure and thus a larger fiber diameter of 520 $\pm$ 34 nm is obtained, as shown in Figure 3b. The fiber diameters of **PHTNF-1** (0.5 mL/h) and **PHTNF-3** (1.5 mL/h) are 168 $\pm$ 20 and 257 $\pm$ 23 nm, respectively. It agrees with the trend of the shell flow rate effect on the fiber diameter, as shown in Figure S2, Supporting Information and summarized in Table 1. The above results suggest that we could control the P3HT ES fiber diameter through the variation of the polymer shell flow rate. All of the prepared P3HT ES nanofibers are smooth and uniform because the high boiling point of ES solvent (chlorobenzene) probably leads to stable cone-jet model during ES process.[30,36]

Figure 3c shows the FE-SEM images of aligned **PHTNF-2** on $SiO_2$/Si substrates after solvent etching and annealing. The inset figure shows that distribution of the angle between the long axis of the fibers and the normal to the edges of two parallel aluminum

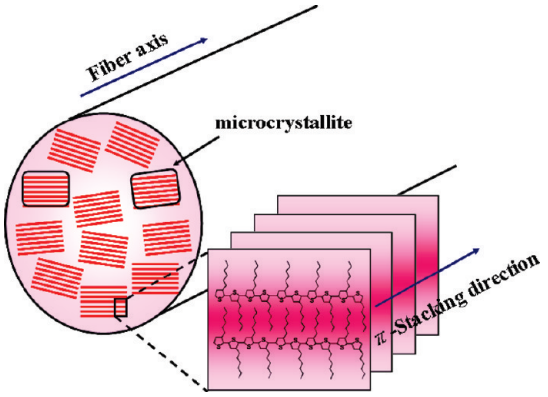


**Figure 6.** Schematic representation on the inner microstructure of single ES P3HT nanofiber.

plates, estimated from more than 50 nanofibers. The distribution of the angle is in a narrow range of 0−10°, suggesting an excellent alignment of the prepared ES nanofibers. As shown in the confocal microscopy image in the inset, the aligned **PHTNF-2** emits uniform red color. By adjusting the collection time through the ES process, we could easily control the numbers of aligned ES nanofibers on OFET device with the top-contact source and drain Au electrodes, as shown in the inset of Figure 3a.

The UV−vis absorption spectra of **PHTNF-1**, **PHTNF-2**, **PHTNF-3**, and **PHTNF-4** are shown in Figure 4a. As shown in the figure, **PHTNF-1** or **PHTNF-2** displays a higher absorption intensity on the shoulder peak (at wavelength ~600 nm) than **PHTNF-3** or **PHTNF-4**, suggesting that the former contains more ordered aggregates associated with interchain $\pi-\pi$ stacking.[24,40] Note that the shoulder peak at 600 nm is assigned to the P3HT crystalline domain.[8] The enhancement in the formation of crystalline domains may be attributed to the stronger stretching force that liquid jet suffered during the ES process, similar to those reported in the literature.[24,25]

The internal structures of the prepared P3HT nanofibers were probed by WAXS. As shown in Figure 4b, three diffraction peaks indexed as (100), (200), and (300) are observable for all nanofibers studied. Furthermore, the (010) diffraction peak due to the $\pi-\pi$ stacking between thiophene moiety is also visible, indicating the presence of crystalline lamellar structure in the nanofibers. It is interesting to note that for **PHTNF-3** and **PHTNF-4** an additional broad peak locating at ca. 3.9 $nm^{-1}$ is found to superpose with the (100) peak. Similar broad peak has been observed in a recent temperature-dependent SAXS study of the melting of P3HT crystallites, where the (100) peak was found to diminish whereas the broad peak beneath it grew during the crystal melting, thereby signifying that the broad peak was associated with amorphous P3HT.[41] Consequently, **PHTNF-3** and **PHTNF-4** which show the broad peak in their WAXS profiles are considered to display lower crystallinty than **PHTNF-1** and **PHTNF-2** which were prepared at lower shell flow rates. The higher crystallinity in the later could be due to higher electrical force per amount of fluid and less concentration in the P3HT core fluid. **PHTNF-1** and **PHTNF-2** may hence be expected to display higher charge mobility.[40−42]

The polarized PL spectra of aligned **PHTNF-2** nanofibers are shown in Figure 5a and 5b. Indeed, the intensity and emission peak wavelength in the PL spectra change significantly with the polarizer direction. All PL spectra with the emission in the perpendicular direction to the nanofibers are red-shifted and

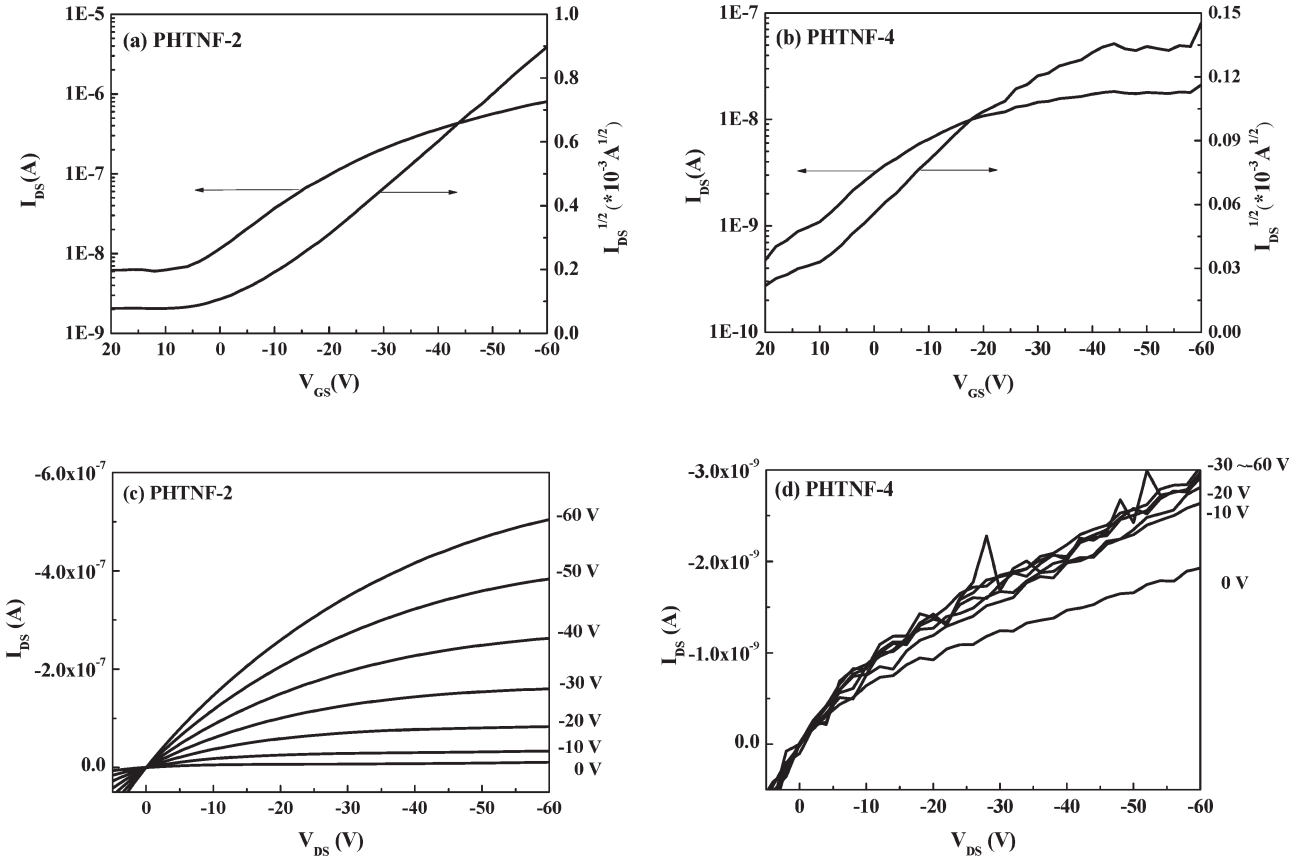


**Figure 7.** (a, b) Transfer characteristics ($-I_{DS}$ and $-I_{DS}^{1/2}$ versus $V_{GS}$ at $V_{DS} = -60$ V) and (c, d) output characteristics of **PHTNF-2** and **PHTNF-4**.

have stronger intensity compared to parallel ones irrespective of whether the exciting light is parallel or perpendicular. For example, the PL polarization ratio ($I_{VHH}/I_{VVV}$) (Figure 5a) reaches 10.8 and the PL peak maximum in the perpendicular axis ($\lambda$ = 662 nm) is red-shifted by 19 nm compared to that of the parallel one ($\lambda$ = 643 nm). Moreover, when exciting with light polarized parallel to the fibers, more light intensity is emitted polarized in the direction perpendicular to the nanofibers (Figure 5b). It suggests that emissive excitons created on shorter conjugated segments may migrate to the longer ones and thus the emitted light is red-shifted and polarized perpendicular to the fiber direction, similar to that reported in the literature.[43] The POM image (shown in Figure S3, Supporting Information) also suggests the birefringence characteristic of **PHTNF-2** and **PHTNF-4** after annealing treatment, indicating the presence of chain orientation and crystallinity.

On the basis of the results of WAXS and polarized PL, a schematic representation of the interior structure of P3HT ES nanofibers is proposed in Figure 6. P3HT undergoes crystallization during the ES process, yielding mcrocrystallites embedded within the nanofiber. The P3HT chains in the crystallites pack into a lamellar structure, with their long chain axis aligning preferentially perpendicular to the long nanofiber axis. The structure shown in Figure 6 is similar to that of 1D supramolecular assembly of P3HT via facile solution processing reported in the literature.[10] However, the prepared P3HT ES nanofibers is an interesting example because the main chain axis of P3HT is actually aligned perpendicular to the fiber axis in spite of the strong elongation force along fiber axis during the ES. Similar result concerning the perpendicular alignment of PTMSDA polymer backbone within ES fibers was also reported by Kwak et al.[26]

*Electrical Properties.* For each type of nanofibers, we measured at least three OFET devices and obtained their carrier mobilities, as shown in Table S1 of the Supporting Information. Although the number of nanofibers on the OFET device is different, it shows the roughly linear relationship with on the current (Figure S4, Supporting Information). It indicates the independence on the carrier mobility of the OFET device with the number of nanofibers, similar to that reported in the literature.[38] As shown in Table S1, Supporting Information, the FET mobility of three **PHTNF-1** OFET devices are $1.44 \times 10^{-1}$, $1.09 \times 10^{-1}$, and $1.78 \times 10^{-1}$ cm$^2$/V·s and the average mobility of $(1.44 \pm 0.35) \times 10^{-1}$ cm$^2$/V·s. All three FET mobility of **PHTNF-1** based devices are on the same order of magnitude ($10^{-1}$ cm$^2$/V·s) and thus the highest mobility ($\mu_{max}$) of $1.78 \times 10^{-1}$ cm$^2$/V·s is reported in Table 1 for comparing with others. Similarly, we used the same ways to measure the mobility of **PHTNF-2**−**PHTNF-8** OFET devices and the results are shown in Table S1 of the Supporting Information.

The output characteristics and transfer characteristics of **PHTNF-2** and **PHTNF-4** nanofibers based OFETs are depicted in Figure 7. The OFET characteristics of **PHTNF-1** and **PHTNF-3** nanofibers based OFETs are shown in Figure S5. As shown in Figure 7, both devices show field-effect characteristics; however, the $-I_{DS}$ of **PHTNF-4** based device seems to be unstable. This maybe contributed to the amorphous P3HT domain presented in the nanofibers that block the hole from hopping. Another possibility is that very little residual PMMA

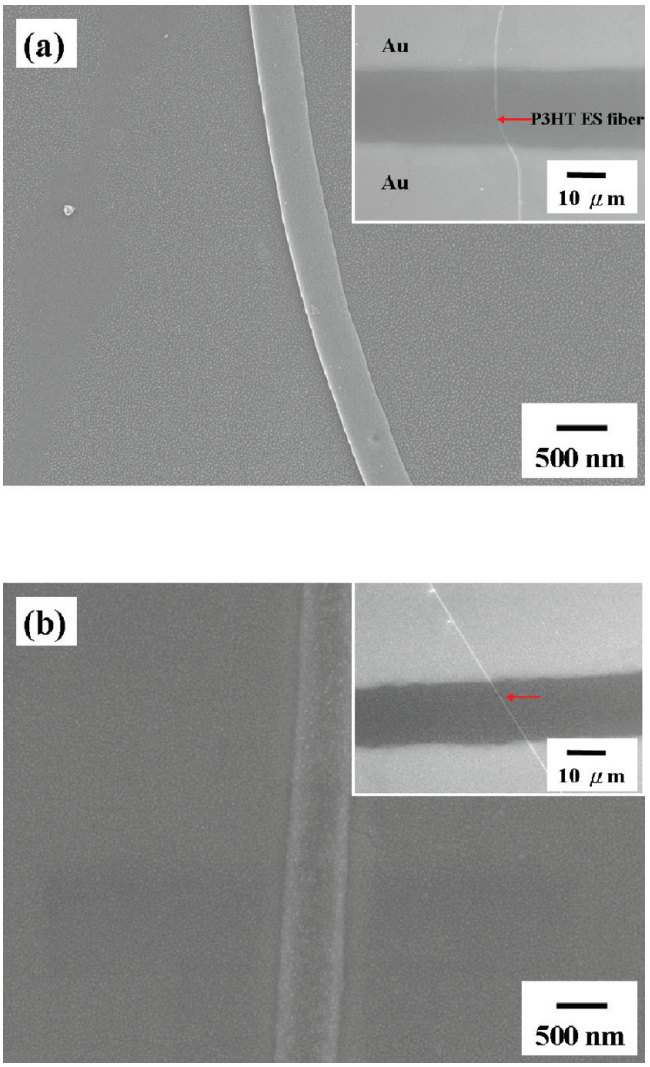


**Figure 8.** FE-SEM images of ES P3HT nanofibers (a) without annealing (**PHTNF-5**) and (b) with annealing at 200 °C (**PHTNF-8**). The inset FE-SEM figures show the typical transistor of the above P3HT nanofibers.

existed in the **PHTNF-4** would cause instability of the source-drain current. The threshold voltage $V_{TH}$ of the devices are determined from a linear relationship between $-I_{DS}^{1/2}$ versus $V_{GS}$ by extrapolation the measured data to -$I_{DS}$ = 0 A. In the saturation region, the modified equation for the current, $I_{DS} = \mu(C/L^2)(V_G - V_{TH})^2$, was used to obtain the charge mobility because a semiconducting cylinder over a planar dielectric layer can be approximated by a coaxial capacitor for nanofiber based OFET devices.[13] The capacitance per unit length $(C/L)$ with respect to the back gate is described by $2\pi\varepsilon\varepsilon_o/\ln(2h/r)$, where $r$, $h$, and $\varepsilon$ are the radius of the fiber, the thickness (200 nm) and average dielectric constant (~2.5) of dielectric layer, respectively. Table 1 lists all electrical properties of P3HT ES nanofiber based OFET devices. From the Table 1, the $\mu_{max}$ of **PHTNF-1**, **PHTNF-2**, **PHTNF-3**, and **PHTNF-4** is 1.78 × $10^{-1}$, 1.92 × $10^{-1}$, 5.93 × $10^{-4}$, and 2.60 × $10^{-4}$ $cm^2/V\cdot s$, respectively, with the corresponding current on/off ratios of 7.54 × $10^2$, 4.45 × $10^4$, 1.17 × $10^3$, and 1.65 × $10^3$. The significant difference on the field-effect mobility by 3 orders of magnitude is attributed to the higher P3HT crystallinity of **PHTNF-1 and**

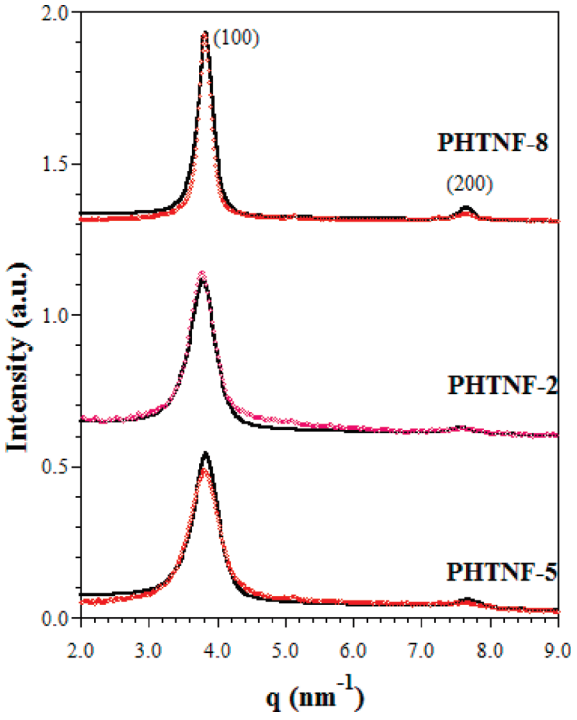


**Figure 9.** XRD patterns of ES P3HT nanofibers of **PHTNF-5**, **PHTNF-2**, and **PHTNF-8**. The solid curves represent the fits by the paracrystalline model of lamellar structure.

**PHTNF-2** prepared at a lower shell flow rate. Note that the obtained fiber diameters of **PHTNF-1**, **PHTNF-2**, **PHTNF-3**, and **PHTNF-4** are 168 ± 20, 131 ± 15, 257 ± 13, and 520 ± 34 nm, respectively. It suggests that the variation on the fiber diameter is mostly within 10%. The hole mobility of **PHTNF-2** using different fiber diameters are 1.92 × $10^{-1}$ $cm^2/V\cdot s$ (131 ± 15 nm), 1.56 × $10^{-1}$ $cm^2/V\cdot s$ (141 ± 21 nm), and 1.34 × $10^{-1}$ $cm^2/V\cdot s$ (158 ± 25 nm), respectively, which suggests the insignificant effect on the mobility by the diameter variation (Table S1, Supporting Information). Furthermore, the obtained hole mobility of the **PHTNF-1 and PHTNF-2** is also higher than the previously reported P3HT nanofiber-based OFET with the hole mobility of 1.7 × $10^{-2}$ $cm^2/V\cdot s$.[13] The significant improvement in the P3HT aligned ES nanofibers in this study is probably due to the following factors: (1) certain level of molecular orientation is developed via the ES process with the help of polymer shell flow, which stabilizes the elongation process with a longer solidification process, rendering P3HT core flow stretched and oriented along fiber axis; (2) the lower P3HT solution concentration compared to the single-capillary ES system results in a slower solidification process and higher electrical-induced force to elongate the fluid jet;[21] (3) the spontaneous carrier generation from the unintentional extrinsic doping by oxygen and moisture could be prevented during the P3HT/PMMA coaxial ES process, resulting in lower off current than that reported previously.[13]

**The Effect of Thermal Annealing Temperature.** The morphology and electronic property OFET devices with P3HT nanofibers prepared from different annealing temperatures were also explored. Parts a and b of Figure 8 shows the SEM images of ES P3HT nanofibers without annealing (**PHTNF-5**) and after annealing at 200 °C (**PHTNF-8**), respectively, while that of

**Table 2. Structural Parameters Obtained from the Fittings of the Experimental WAXS Profiles of PHTNF-2, PHTNF-5, and PHTNF-8 by the Lamellar Structure Model**

| sample | D[a] (nm) | crystalline domain size (nm) | g[b] | l[c] (nm) | $\sigma_L$[d] |
|---|---|---|---|---|---|
| **PHTNF-1** | 1.62 | 5.75 | 0.17 | 0.48 | 0.055 |
| **PHTNF-2** | 1.65 | 7.12 | 0.14 | 0.50 | 0.048 |
| **PHTNF-5** | 1.63 | 7.11 | 0.17 | 0.53 | 0.075 |
| **PHTNF-6** | 1.62 | 6.73 | 0.13 | 0.47 | 0.052 |
| **PHTNF-7** | 1.65 | 9.04 | 0.11 | 0.42 | 0.036 |
| **PHTNF-8** | 1.64 | 12.03 | 0.12 | 0.51 | 0.032 |

[a] Interlamellar distance corresponding to the sum of the thickness of the backbone and the side-chain layer of P3HT. [b] Ratio of the mean displacement of the lattice points to the interlamellar distance. [c] Average thickness of the backbone layer. [d] Polydispersity of the backbone layer thickness given by the ratio of the standard deviation of the distribution to the average thickness.

annealing at 100 °C (**PHTNF-2**) has been shown in Figure 3a. P3HT ES nanofibers annealed at 50 °C (**PHTNF-6**) and 150 °C (**PHTNF-7**) are exhibited in Figure S6 of the Supporting Information. The fiber diameters of **PHTNF-5**, **PHTNF-6**, **PHTNF-2**, **PHTNF-7**, and **PHTNF-8** are 325 ± 21, 124 ± 10, 131 ± 15, 442 ± 31, and 421 ± 33 nm, respectively. The initial decrease on the fiber diameter up to 100 °C is probably due to the solvent evaporation. However, the ES fibers are gradually flattened as the annealed temperature is above 100 °C and leads to a broader diameter. The thickness of **PHTNF-2** and **PHTNF-8** estimated from AFM cross section image (Figure S7) are 174 nm (100 °C) and 74 nm (200 °C), which also confirms the gradually flattened fiber structure by annealing from 100 to 200 °C, respectively. Such flattened nanofiber morphology (Figure 8b) could reduce the geometrical confinement on the P3HT and affect the carrier mobility.

Figure 9 shows the WAXS patterns of **PHTNF-5**, **PHTNF-2**, and **PHTNF-8** and those of **PHTNF-6** and **PHTNF-7** are in Figure S8 of the Supporting Information. As shown in the Figure 9, the width of the (100) peak decreases with increasing annealing temperature; besides, the small broad peak beneath the (100) peak appears to vanish upon the annealing. The results demonstrate that the postannealing is able to increase the P3HT crystallite size and crystallinity. The increase of crystalline domain size is confirmed quantitatively by fitting the WAXS profiles using the scattering function of lamellar structure developed by Förster et al.[43] This model takes into account lamellar thickness distribution, distortion of interlamellar distance, grain size and peak shape which varies analytically between Lorentzian and Gaussian functions. The fitted results are displayed by the solid curves in Figure 9 and the values of the structure parameters obtained from the fit are listed in Table 2. It can be seen from Table 2 that the crystalline domain size increases from ca. 7 nm in the unannealed nanofiber (i.e., **PHTNF-5**) to ca. 12 nm in the nanofiber subjected to annealing at 200 °C (i.e., **PHTNF-8**). The polarized PL spectra of aligned **PHTNF-5**, **PHTNF-2**, and **PHTNF-8** with emission polarization perpendicular ($I_{VOH}$) and parallel ($I_{VOV}$) to the nanofiber axis show polarization anisotropy as shown in parts a−c of Figure 10, respectively. Using polarized PL spectra to explore polymer chain orientation had been reported in the literatures.[26,36,44] With exciting at 550 nm by unpolarized light source, the polarization ratios (perpendicular: parallel) of **PHTNF-5**, **PHTNF-2**, and **PHTNF-8** attain 2.27, 2.72, and

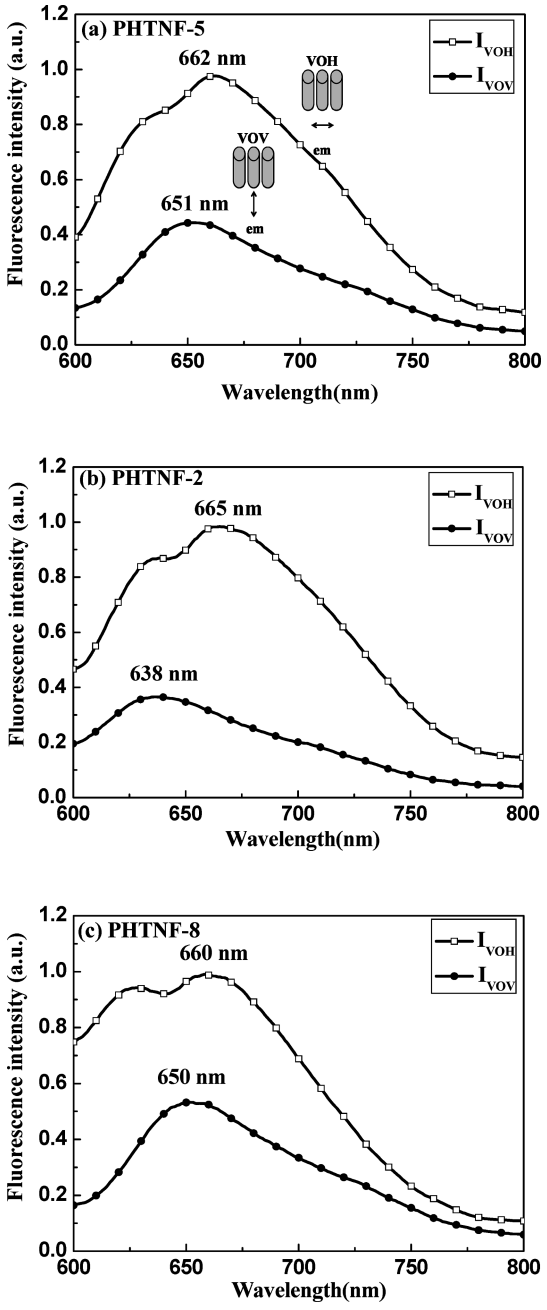


**Figure 10.** Polarized Photoluminescence of aligned ES P3HT nanofibers (**PHTNF-5**, **PHTNF-2**, and **PHTNF-8**) with unpolarized exciting light, and emission collected polarized perpendicular ($I_{VOH}$) and parallel ($I_{VOV}$) to fiber axis.

1.89, respectively. **PHTNF-2** exhibits a higher polarization ratio which indicates a better P3HT orientation structure than that of **PHTNF-5** and **PHTNF-8**. Furthermore, the shifts of PL maximum emission peak between perpendicular and parallel are 11, 27, and 10 nm for **PHTNF-5**, **PHTNF-2**, and **PHTNF-8**, respectively. The aligned P3HT main chains are highly elongated, densely packed, perpendicular to the long **PHTNF-2** axis, leading to the more extensive $\pi$-electron delocalization and the red-shifted PL maximum. According to the above results, it obviously indicates chain orientation of P3HT within ES nanofibers have the following order: **PHTNF-2** > **PHTNF-5** > **PHTNF-8**,

suggesting the importance of using suitable annealing temperature. The above results suggests that crystallite grains exhibit orientational direction along P3HT ES nanofiber axis and high crystallinity could be obtained using a suitable annealing treatment.

*Electrical Properties.* The transfer characteristics and the output characteristics of **PHTNF-5** ∼ **PHTNF-8** OFETs are shown in Figure S9, Supporting Information, and the corresponding electronic properties are summarized in Table 1. Note that that numbers of **PHTNF-5**−**8** nanofibers in the OFET devices are 4, 5, 3, and 3, respectively. From Table 1, the $\mu_{max}$ of **PHTNF-5**, **PHTNF-6**, **PHTNF-2**, **PHTNF-7**, and **PHTNF-8** is $1.51 \times 10^{-4}$, $5.56 \times 10^{-2}$, $1.92 \times 10^{-1}$, $4.57 \times 10^{-2}$ and $4.88 \times 10^{-3}$ $cm^2/V \cdot s$, respectively. As shown above, the mobility of the prepared P3HT nanofibers increases steadily for the annealed temperatures up to 100 °C due to the enhanced P3HT crystallinity. However, it drops abruptly as the annealed temperatures over 100 °C since the cylindrical nanofibers become flattened and lose the originally geometrical confinement by the melting process.[41] Also, such morphological change is accompanied by the reduction of orientation of the noncrystalline P3HT chains within fiber induced initially by the ES process because of conformational relaxation. The annealing temperature significantly affected the microstructure of P3HT, resulting in variation of the charge-carrier mobility. Recent study[41] suggested that the higher ordered structure was obtained at the annealing temperature around 100 °C but the crystallinity was significantly reduced for the annealing temperature above 150 °C. Such conclusion is similar to our result, due to the loss of the geometrical confinement.

The dimension of the nanofibers is relatively limited in comparison with that of the spin-coated film.[45] Also, the strong stretching force and the geometrical confinement associated with the ES process could induce the orientation of polymer chains along the long axis of fiber. Such geometrical effect could affect the carrier mobility of the P3HT. Although it has been found that a certain level of molecular orientation can be developed via the ES process, there is relatively poor crystalline order along the fibrillar axis because of the rapid solidification of a fluid jet, in comparison with the process of spin-coating or drop-casting.[21] Therefore, annealing is an essential process to improve the crystallinity. However, the relaxation of polymer chains induced by a higher annealing temperature might destroy the initial orientation of polymer chains within the ES nanofibers, which inhibits charge-carrier hopping through $\pi-\pi$ stacking between polymer chains. The experimental results demonstrated that both the orientation of the noncrystalline chains and crystallinity of the P3HT in the ES nanofibers affect the OFET mobility significantly.

## CONCLUSIONS

We have successfully prepared aligned P3HT ES nanofibers for OFET applications by two-fluid coaxial electrospinning (ES) technique. Higher crystallinity and preferred orientation of P3HT within ES nanofibers were evidenced by WAXS, optical absorption and polarized photoluminescence at a lower shell flow rate (such as 1.0 mL/h), which is attributed to the strong electrical force along fiber axis. As a result, a significant increase of the field-effect mobility up to 3 orders of magnitude ($1.92 \times 10^{-1}$ $cm^2/V \cdot s$) than that at higher shell flow rate (2.0 mL/h). On the other hand, the experimental results also indicated that annealing process was favorable for improving the P3HT crystallinity within the ES nanofibers. However, the geometrical confinement and orientation of noncrystalline chains provided by ES process might be reduced and thus a lower OFET mobility was obtained. The experimental results suggested the importance of the process parameters (the shell flow rate and thermal annealing temperature) on the morphology of P3HT nanofibers and their electrical device characteristics.

## ASSOCIATED CONTENT

**Supporting Information.** FE-SEM images of aligned as-spun coaxial **PHTNF-2** and **PHTNF-4** fibers, FE-SEM images of **PHTNF-1** and **PHTNF-3**, birefringence of **PHTNF-2** and **PHTNF-4**, transfer characteristics ($I_{DS}$ and $I_{DS}^{1/2}$ versus $V_{GS}$ at $V_{DS} = -60$ V) and output characteristics of **PHTNF-1** and **PHTNF-3**, variation of the on-current with the fiber number of **PHTNF-2**, FE-SEM images of **PHTNF-6** and **PHTNF-7**, AFM images of **PHTNF-2** and **PHTNF-8**, XRD patterns of **PHTNF-7** and **PHTNF-6**, transfer characteristics and output characteristics of **PHTNF-5**, **PHTNF-6**, **PHTNF-2**, **PHTNF-7**, and **PHTNF-8**, electrical properties and the average mobility of the P3HT ES nanofibers based OFET devices prepared at different process parameters. This material is available free of charge via the Internet at http://pubs.acs.org.

## AUTHOR INFORMATION

### Corresponding Author

*E-mail: (W.-C.C.) chenwc@ntu.edu.tw; (H.-L.C.) hslchen@mx.nthu.edu.tw.

### Author Contributions

⊥These authors equally contributed to this work.

## ACKNOWLEDGMENT

The financial support from National Science Council of Taiwan, Ministry of Economics Affairs of Taiwan, and National Taiwan University Excellent Research program are highly appreciated. We thank the technical assistance of Mr. Yu-Chen Chiu and Ping Tzeng.

## REFERENCES

(1) Coakley, K. M.; McGehee, M. D. *Chem. Mater.* **2004**, *16*, 4533.
(2) Huynh, W. U.; Dittmer, J. J.; Alivisatos, A. P. *Science* **2002**, *295*, 2425.
(3) Li, G.; Shrotriya, V.; Huang, J.; Yao, Y.; Moriarty, T.; Emery, K.; Yang, Y. *Nat. Mater.* **2005**, *4*, 864.
(4) Li, S. S.; Tu, K. H.; Lin, C. C.; Chen, C. W.; Chhowalla, M. *ACS Nano* **2010**, *4*, 3169.
(5) Yang, H.; Shin, T.; Yang, L.; Cho, K.; Ryu, C.; Bao, Z. *Adv. Funct. Mater.* **2005**, *15*, 671.
(6) Zen, A.; Pflaum, J.; Hirschmann, S.; Zhuang, W.; Jaiser, F.; Asawapirom, U.; Rabe, J.; Scherf, U.; Neher, D. *Adv. Funct. Mater.* **2004**, *14*, 757.
(7) Aryal, M.; Trivedi, K.; Hu, W. *ACS Nano* **2009**, *3*, 3085.
(8) Oosterbaan, V. D.; Bolsee, J.-C.; Gadisa, A.; Vrindts, V.; Bertho, S.; D'Haen, J.; Cleij, T. J.; Lutsen, L.; McNeil, C. R.; Thomsen, L.; Manca, J. V.; Vanderzande, D. *Adv. Funct. Mater.* **2010**, *20*, 792.
(9) Briseno, A. L.; Mannsfeld, S. C. B.; Jenekhe, S. A.; Bao, Z.; Xia, Y. *Mater. Today* **2008**, *11*, 38.
(10) Kim, D.; Han, J.; Park, Y.; Jang, Y.; Cho, J.; Hwang, M.; Cho, K. *Adv. Mater.* **2006**, *18*, 719.
(11) Merlo, J. A.; Frisbie, C. D. *J. Phys. Chem. B* **2004**, *108*, 19169.

(12) Samitsu, S.; Shimomura, T.; Heike, S.; Hashizume, T.; Ito, K. *Macromolecules* **2010**, *43*, 7891.
(13) Lee, S.; Moon, G. D.; Jeong, U. *J. Mater. Chem.* **2009**, *19*, 743.
(14) Liu, H. Q.; Reccius, C. H.; Craighead, H. G. *Appl. Phys. Lett.* **2005**, *87*, 253106.
(15) Gonzalez, R.; Pinto, N. J. *Synth. Met.* **2005**, *151*, 275.
(16) Reneker, D. H.; Chun, I. *Nanotechnology* **1996**, *7*, 216.
(17) Li, D.; Xia, Y. *Adv. Mater.* **2004**, *16*, 1151.
(18) Wang, C.; Chien, H. S.; Hsu, C. H.; Wang, Y. C.; Wang, C. T.; Lu, H. A. *Macromolecules* **2007**, *40*, 7973.
(19) Ma, M.; Krikorian, V.; Yu, J. H.; Thomas, E. L.; Rutledge, G. C. *Nano Lett.* **2006**, *6*, 2969.
(20) Greiner, A.; Wendorff, J. H. *Angew. Chem., Int. Ed.* **2007**, *46*, 5670.
(21) Inai, R.; Kotaki, M.; Ramakrishna, S. *Nanotechnology* **2005**, *16*, 208.
(22) Kakade, M. V.; Givens, S.; Gardner, K.; Lee, K. H.; Chase, D. B.; Rabolt, J. F. *J. Am. Chem. Soc.* **2007**, *129*, 2777.
(23) Li, C.; Vepari, C.; Jin, H. J.; Kim, H. J.; Kaplan, D. L. *Biomaterials* **2006**, *27*, 3115.
(24) Babel, A.; Li, D.; Xia, Y. N.; Jenekhe, S. A. *Macromolecules* **2005**, *38*, 4705.
(25) Li, D.; Babel, A.; Jenekhe, S.; Xia, Y. *Adv. Mater.* **2004**, *16*, 2062.
(26) Kwak, G.; Fukao, S.; Fujiki, M.; Sakaguchi, T.; Masuda, T. *Chem. Mater.* **2006**, *18*, 5537.
(27) Yoon, J.; Chae, S. K.; Kim, J. M. *J. Am. Chem. Soc.* **2007**, *129*, 3038.
(28) Kuo, C. C.; Lin, C. H.; Chen, W. C. *Macromolecules* **2007**, *40*, 6959.
(29) Kuo, C. C.; Wang, C. T.; Chen, W. C. *Macromol. Symp.* **2009**, *279*, 41.
(30) Wang, C. T.; Kuo, C. C.; Chen, H. C.; Chen, W. C. *Nanotechnology* **2009**, *20*, 37560.
(31) Kuo, C. C.; Tung, Y. C.; Chen, W. C. *Macromol. Rapid Commun.* **2010**, *31*, 65.
(32) Kameoka, J.; Orth, R.; Yang, Y. N.; Czaplewski, D.; Mathers, R.; Coates, G. W.; Craighead, H. G. *Nanotechnology* **2003**, *14*, 1124.
(33) Doshi, J.; Reneker, D. H. *J. Electrost.* **1995**, *35*, 151.
(34) Theron, A.; Zussman, E.; Yarin, A. L. *Nanotechnology* **2001**, *12*, 384.
(35) Li, D.; Wang, Y.; Xia, Y. *Nano Lett.* **2003**, *3*, 1167.
(36) Kuo, C. C.; Wang, C. T.; Chen, W. C. *Macromol. Mater. Eng.* **2008**, *293*, 999.
(37) Liu, Y.; Zhang, X.; Xia, Y.; Yang, H. *Adv. Mater.* **2010**, *22*, 2454.
(38) Lee, S. W.; Lee, H. J.; Choi, J. H.; Koh, W. G.; Myoung, J. M.; Hur, J. H.; Park, J. J.; Cho, J. H.; Jeong, U. *Nano Lett.* **2009**, *10*, 347.
(39) Chang, J. F.; Sun, B.; Breiby, D. W.; Nielsen, M. M.; Solling, T. I.; Giles, M.; McCulloch, I.; Sirringhaus, H. *Chem. Mater.* **2004**, *16*, 4772.
(40) Kline, R. J.; McGehee, M. D.; Kadnikova, E. N.; Liu, J.; Frechet, J. M. J.; Toney, M. F. *Macromolecules* **2005**, *38*, 3312.
(41) Wu, Z. Y.; Petzold, A.; Henze, T.; Thurn-Albrecht, T.; Lohwasser, R. H.; Sommer, M.; Thelakkat, M. *Macromolecules* **2010**, *43*, 4646.
(42) Sethuraman, K.; Ochiai, S.; Kojima, K.; Mizutani, T. *Appl. Phys. Lett.* **2008**, *92*, 183302.
(43) Förster, S.; Timmann, A.; Schellbah, C.; Meyer, A.; Funari, S. S.; Mulvaney, P.; Knott, R. *J. Phys. Chem. B* **2005**, *109*, 1347.
(44) Nguyen, T. Q.; Wu, J.; Doan, V.; Schwartz, B. J.; Tolbert, S. H. *Science* **2000**, *288*, 652.
(45) Chang, C. C.; Pai, C. L.; Chen, W. C.; Jenekhe, S. A. *Thin Solid Films* **2005**, *479*, 254.